SANDIA REPORT

SAND2004-3482
Unlimited Release
Printed July 2004

An Evaluation of the PENCURV Model for Penetration Events in Complex Targets

Todd P. Broyles

Prepared by
Sandia National Laboratories
Albuquerque, New Mexico 87185 and Livermore, California 94550

Sandia is a multiprogram laboratory operated by Sandia Corporation,
a Lockheed Martin Company, for the United States Department of Energy's
National Nuclear Security Administration under Contract DE-AC04-94AL85000.

Issued by Sandia National Laboratories, operated for the United States Department of Energy by Sandia Corporation.

Available to DOE and DOE contractors from
U.S. Department of Energy
Office of Scientific and Technical Information
P.O. Box 62
Oak Ridge, TN 37831

Telephone: (865)576-8401
Facsimile: (865)576-5728
E-Mail: reports@adonis.osti.gov
Online ordering: http://www.osti.gov/bridge

Available to the public from
U.S. Department of Commerce
National Technical Information Service
5285 Port Royal Rd
Springfield, VA 22161

Telephone: (800)553-6847
Facsimile: (703)605-6900
E-Mail: orders@ntis.fedworld.gov
Online order: http://www.ntis.gov/help/ordermethods.asp?loc=7-4-0#online

SAND 2004-3482
Unlimited Release
Printed July 2004

An Evaluation of the PENCURV Model for Penetration Events in Complex Targets

Todd P. Broyles
Weapon Knowledge Management Dept.
Sandia National Laboratories
P. O. Box 5800
Albuquerque, New Mexico 87185-0632

Abstract

Three complex target penetration scenarios are run with a model developed by the U. S. Army Engineer Waterways Experiment Station, called PENCURV. The results are compared with both test data and a Zapotec model to evaluate PENCURV's suitability for conducting broad-based scoping studies on a variety of targets to give first order solutions to the problem of G-loading. Under many circumstances, the simpler, empirically based PENCURV model compares well with test data and the much more sophisticated Zapotec model. The results suggest that, if PENCURV were enhanced to include rotational acceleration in its G-loading computations, it would provide much more accurate solutions for a wide variety of penetration problems. Data from an improved PENCURV program would allow for faster, lower cost optimization of targets, test parameters and penetration bodies as Sandia National Laboratories continues in its evaluation of the survivability requirements for earth penetrating sensors and weapons.

Acknowledgements

I would like to thank several individuals who contributed to this effort through providing required data, and engaging in critical discussion and review of written materials. I would particularly like to thank Dr. Paul Yarrington and Dr. David Gardner for handing me this project and giving me the opportunity to make a substantive contribution during my time here at Sandia National Laboratories. Thanks to Dr. Marlin Kipp, Joe Crepeau and Dr. Jeromy Hollenshead for their technical contributions and discussions. Finally, I wish to thank committee members Dr. John Hogan and Professor Hal Walling for all their help throughout this degree program and their continued unwavering support of the Weapon Interns.

The original of this report was an independent study submitted to the Department of Engineering Mechanics and the Graduate School of the New Mexico Institute of Mining and Technology, Socorro, New Mexico, in partial fulfillment of the requirements for the degree of Master of Science in Engineering Mechanics, May 2004.

Table of Contents

List of Figures

List of Tables

Page

List of Abbreviations

CRH	Caliber Radius Head
CTH	A Sandia National Laboratories developed Eulerian finite difference code capable of modeling strong shock physics events
JANUS	A massively parallel computing platform at Sandia National Laboratories
HDBT	Hardened Deeply Buried Target
LDRD	Laboratory Directed Research and Development
LSG-x	Test names given to the four Complex Target Tests
PC	Personal Computer
PENCURV	A US Army Corps of Engineers developed empirical penetration code capable of modeling penetration events into curvilinear materials
PLOTDATA	A data processing package developed at Sandia National Laboratories
Pronto 3D	A Lagrangian program designed to analyze the three-dimensional response of solid bodies subjected to transient dynamic loading
QT	A massively parallel computing platform at Sandia National Laboratories
SAMPLL	Simplified Analytical Model of Penetration with Lateral Loading – An empirical penetration code capable of modeling penetration events into parallel, laterally infinite rock strata
SNL	Sandia National Laboratories
UCS	Unconfined Compressive Strength
Zapotec	A program designed to solve complex problems by utilizing both the Eulerian code CTH and the Lagrangian code Pronto

An Evaluation of the PENCURV Model for Penetration Events in Complex Targets

1. Introduction

The military has long been interested in the field of penetration mechanics. Back in the 1700s, artillery fire was becoming an increasingly effective weapon of war. As such, engineers were very interested in calculating the thickness of earthen embankments required to adequately protect their troops and equipment [1]. By World War II, both the Germans and the Allies were designing and building penetrator weapons [2]. The interest in penetration mechanics continues today as better models are sought that will more accurately describe penetration events.

Along with technological advances, the worldwide geopolitical climate has changed significantly over the past decade. As belligerent countries and/or ideological groups have come to see the accuracy and supremacy of American air power, they have commenced burying their command and control structures and other high value assets deeper and deeper underground. While the military's strategy and tactics are changing in response to this, these facts highlight the need for new sensors and weapons to be employed in new ways and on new sets of targets.

Over the last 40 years, Sandia National Laboratories has been interested in earth penetrator technology, especially to take advantage of coupling energy into the ground. Perhaps the watershed research in terradynamics was in the development of penetration equations for soil and rock published by Young [1]. These empirical equations were based on an extensive experimental database of full-scale tests into a variety of rock and soil targets. They allowed for the estimation of depth of penetration with inputs of the rock penetrability index, penetrator weight, nose performance coefficient, penetrator cross-sectional area, and penetrator velocity.

Over the years, there have been several modifications and improvements to Young's original work. Young [3] introduced a method of incorporating more complex penetrator geometries such as terrabrakes and detachable after-bodies. He also employed a technique for modeling layered geology targets. In 1988, Young [4] summarized additional equations developed to describe penetrability in specific target environments such as ice and concrete. Later, Forrestal, *et al.* [5] derived their own equation for penetration depth into concrete targets. Their equation uses a single, dimensionless empirical constant that depends only on the unconfined compressive strength of the target.

The techniques previously mentioned are valuable for penetration depth calculations, but other parameters that describe the penetration event are also items of keen interest. Of special concern is the G-loading experienced by the penetrator during the impact event.

Since an earth penetrator is ideally designed for a wide array of target geologies, the great engineering challenge is to design a sensor or weapon that will be able to survive the axial and lateral G-loading that will take place during penetration. These G-loads depend on a number of factors such as penetrator geometry, penetrator mass properties, penetrator velocity, angle of impact, angle of attack, rock properties, and non-uniform target geology. All of these variables can create asymmetric forces acting on the penetrator, thereby inducing large lateral loading. Of particular interest is the effect of non-uniform rock properties. For instance, what would be the sensitivity of an earth penetrator to buried obstacles such as a hard granitic boulder surrounded by a much softer sedimentary matrix?

Once these G-loading environments are known, components and systems can be designed, built, and tested to survive these environments, thus ensuring the functionality of the system after the penetration event. Both axial and lateral loads are of interest. But the major concern for system survival is with the lateral loads, since they can cause severe component lateral accelerations and case bending strains.

Preliminary analysis has shown that an earth penetrator, under certain conditions, would indeed exhibit some sensitivity to near-surface boulders and other shallow buried features which exhibit material strength contrasts of sufficient magnitude. But what exactly is "near-surface", and what is the minimum size boulder and material contrast that would likely cause unacceptable damage to the penetrator?

These issues are being investigated as part of a Sandia National Laboratories Grand Challenge, Laboratory Directed Research and Development (LDRD) project entitled "Near Real-Time Site Characterization for Assured Hard Deeply Buried Target (HDBT) Defeat". The vision of this project is to "perform research and development for the key technologies for a sensor system that will assure success of a nuclear earth penetrator weapon strike on an underground strategic target through rapid site characterization and optimal aim point selection" [6]. In other words, to maximize the probability of survival for an earth-penetrating weapon, the desire is to quickly characterize the surface and near-surface geologic features for homogeneity and penetrability. The goal, then, is to find the "sweet spots" in the geology that can be targeted for subsequent earth penetrator employment.

Two of the significant unknowns that could jeopardize the survivability of a penetrator need to be quantified. First, the maximum allowable size of a near-surface inclusion must be calculated. Second, the maximum allowable rock strength contrast between two adjacent rock masses must be calculated. It should be noted that these variables are interrelated. For instance, if we have a smaller strength contrast, we can tolerate a larger boulder.

These are difficult questions and, given the range of variables involved, such as geologic environments and penetrator geometries, the only feasible way to address them is through conducting a lengthy series of computer simulations that can account for these variables. Such an approach is necessary to adequately scope out all plausible scenarios. The next step, then, is to determine what simulation programs are best suited for this type of investigation.

2. Research Approach

Several software packages have been developed over the years to model penetration mechanics. A program first written in 1982 is the Simplified Analytical Model of Penetration with Lateral Loading (SAMPLL) [7]. It was created primarily as a tool to model axial and lateral G-loads. SAMPLL combines empirical loading algorithms with user defined parameters, such as penetrator geometry and mass properties, impact angle, and angle of attack to calculate the resulting kinematics. It also possesses an option for estimating penetrator damage or failure. The program allows for complex axisymmetric penetrator shapes, but assumes a rigid body. An added feature permits "point" instrumentation that lets the user calculate G-loads for particular points in the penetrator. A significant limitation, however, is that target geology may only be defined as parallel, laterally infinite strata of constant thickness. It is therefore unsuitable to the purposes of this study.

Another package, PENCURV, is a PC-based penetration modeling program developed by the Geotechnical and Structures Laboratory at the Engineer Research and Development Center, US Army Corps of Engineers [8]. It has the advantage of possessing a three-dimensional projectile penetration code that calculates the penetration of a rigid, non-spinning projectile into a target that may contain curvilinear material layers. PENCURV allows creation of any axisymmetric penetrator geometry along with the desired center of gravity and moments of inertia. To model a given target geology, PENCURV uses two primary algorithms for generating stress equations, both of which are empirically derived. One is used to model hard rock and the other is for soft rock. A distinct advantage for PENCURV is that simulations generally take only a few seconds to run on a typical PC.

Yet another code that can be used to model penetration events is called CTH [9]. Developed at Sandia National Laboratories, CTH is an Eulerian finite difference code capable of modeling multidimensional, multi-material, large deformation, strong shock wave physics events [10]. It can simulate hydrodynamic behavior via several different equation-of-state models. This permits treatment of complex material behavior such as solid-solid phase transitions, and melting and vaporization. CTH can also model elastic-plastic behavior with a number of different algorithms. It also contains a model for fracture. These last two phenomena are the most important for the pressure regimes that are encountered during penetration events.

While CTH has advantages, the penetrator is generally best modeled using a finite element approach such as that found in Pronto 3D. Pronto 3D is a Lagrangian program designed to analyze the three-dimensional response of solid bodies subjected to transient dynamic loading [11]. Zapotec, yet another program, combines the strengths of both CTH and Pronto 3D. It is designed to solve problems that prove difficult using Eulerian or Lagrangian methods alone. For instance, in earth penetration problems, the soil is best modeled using Eulerian methods due to its large deformation. Conversely, the penetrator is best modeled using Lagrangian methods since structural response is the primary interest [12].

While programs such as Zapotec have been demonstrated as valuable modeling tools, it may take considerable computer time to execute a particular scenario in the code. For instance, the Zapotec model discussed later in this paper took about 1.5 days of clock time per 2 ms of calculation time. That particular simulation would require about 800 processors on JANUS or 12 processors on QT. It follows that, for studies which require a large variety of target models, faster lower fidelity modeling platforms should be considered.

Therefore, the primary thrust of this study is to test the suitability of PENCURV for conducting broad-based scoping studies on a variety of targets to give first order solutions to the problem of G-loading. This study will be accomplished using four test shots. All of the tests were designed as vertical impact shots fired at a nominal velocity of 200 m/s (656 ft/s). The difference between them was in the targets. One target was a homogeneous grout and the other three contained a hard inclusion buried within the softer grout matrix.

3. Building the Homogeneous Grout Model

Four vertical gun tests, named LSG-1, LSG-2, LSG-3, and LSG-4, were conducted for this analysis in September 2003. The projectiles used were identical to those used by Frew in earlier tests into concrete [13]. They were 20.4 inches (51.8 cm) long, 3.0 inches (7.62 cm) in diameter, and weighed 28.9 pounds (13.1 kg). The cases were made of heat-treated 4340 steel. They had a 3.0 CRH nose and a very slight flare aft. Inside, data recorders and a battery pack were mounted to record acceleration data in the axial, pitch, and yaw directions. A cross-section of the penetrator is shown in Figure 1.

The penetrators were fired from a vertically mounted gas gun into the four targets (Figure 2). They ranged in speed from 648.8 ft/s (197.8 m/s) for LSG-4 to 661.9 ft/s (201.7 m/s) for LSG-3. Figure 3 shows a penetrator with a sabot wrapped around it prior to firing as well as the top of one of the targets after a test. The targets were all right circular cylinders in shape. They had diameters of 7.0 feet (2.13 m) and were all 4.0 feet (1.22 m) thick. The LSG-1 target consisted of a homogeneous low-strength grout. LSG-1 was performed to baseline the penetrability of the grout. The targets for LSG-2 and LSG-3 were identical to LSG-1 except that they each had an Indiana limestone rod embedded in the top center of the target. The limestone rods were right circular cylinders and were 12.0 inches (30.5 cm) long by 3.0 inches (7.62 cm) in diameter. They were positioned horizontally in an East-West direction as seen in Figure 4. For LSG-4, a 3.0-inch (7.62-cm) diameter sphere composed of 6061 T6 aluminum was embedded in the top center of the target in place of the limestone rod. The nominal impact geometry can be seen in Figure 5. It should be noted that the nominal impact points for LSG-2, -3 and -4 were defined directly over the vertical edge of the inclusions to inflict maximum lateral G-loading on the penetrator. The initial conditions for LSG-1, -2, -3 and -4 are given in Tables 1–4.

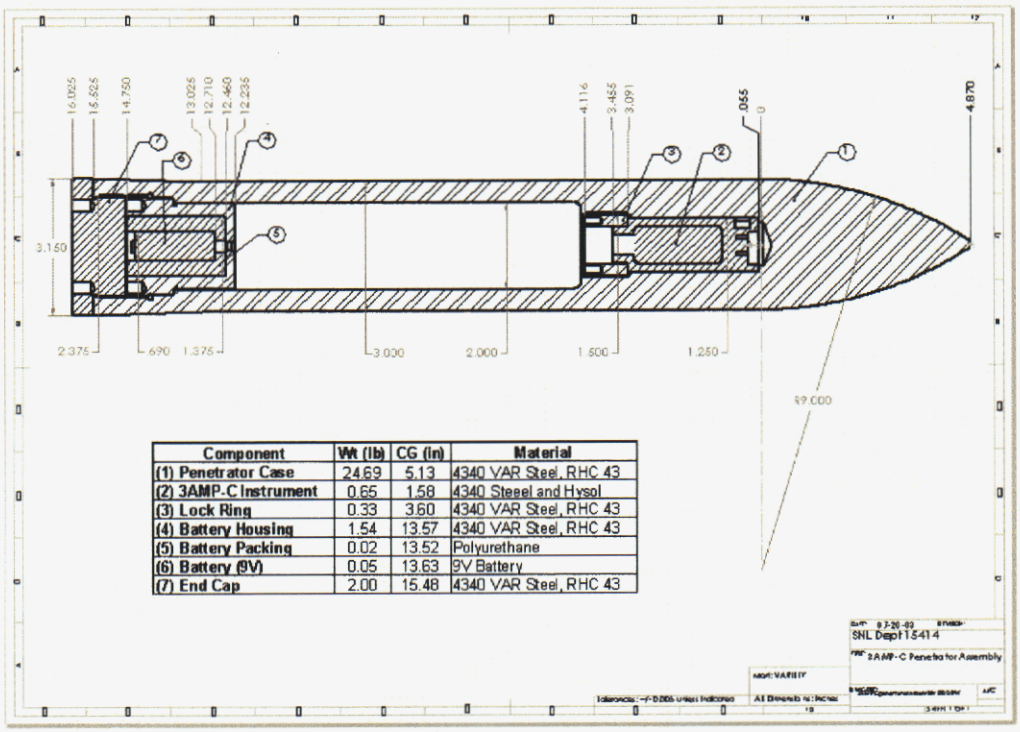

Component	Wt (lb)	CG (in)	Material
(1) Penetrator Case	24.69	5.13	4340 VAR Steel, RHC 43
(2) 3AMP-C Instrument	0.65	1.58	4340 Steeel and Hysol
(3) Lock Ring	0.33	3.60	4340 VAR Steel, RHC 43
(4) Battery Housing	1.54	13.57	4340 VAR Steel, RHC 43
(5) Battery Packing	0.02	13.52	Polyurethane
(6) Battery (9V)	0.05	13.63	9V Battery
(7) End Cap	2.00	15.48	4340 VAR Steel, RHC 43

Figure 1. Cross Section of the Penetrator Case [13]

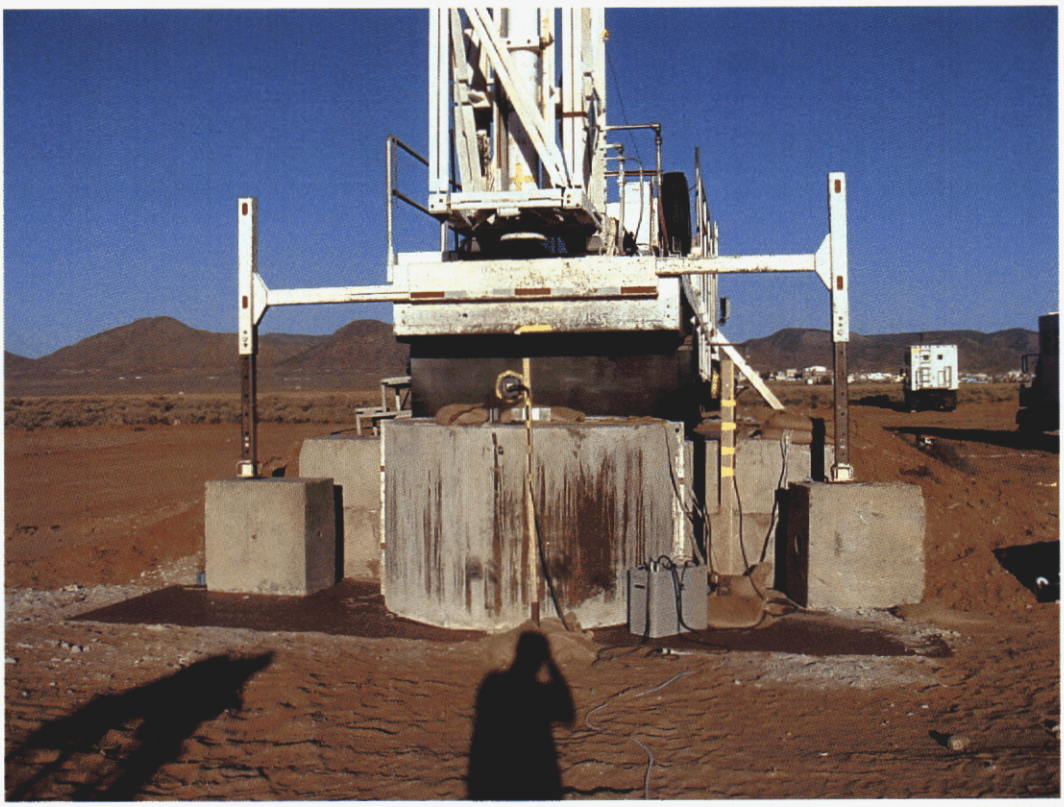

Figure 2. Vertical Gas Gun Test Configuration at SNL

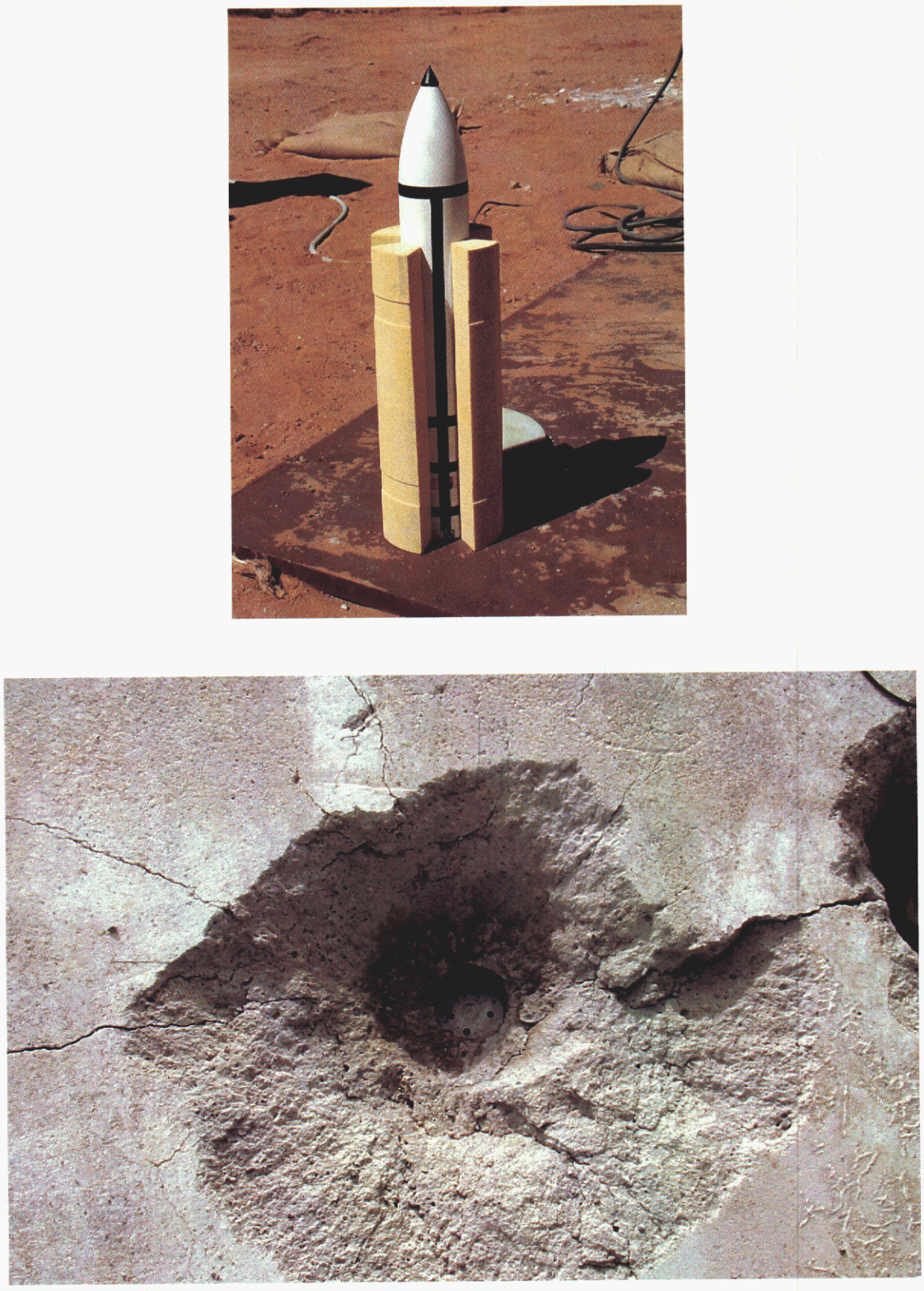

Figure 3. Pre-Test Penetrator (Upper Photograph) and Post-Test Penetrator Buried in Target (Lower Photograph)

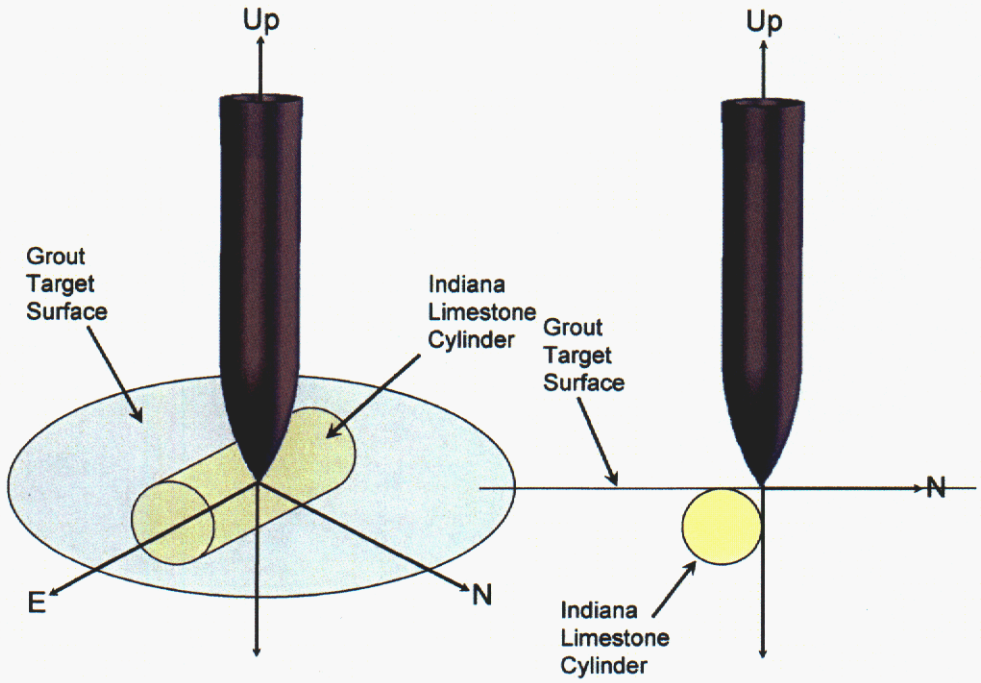

Figure 4. Nominal Impact Geometry for LSG-2 and LSG-3 [14]

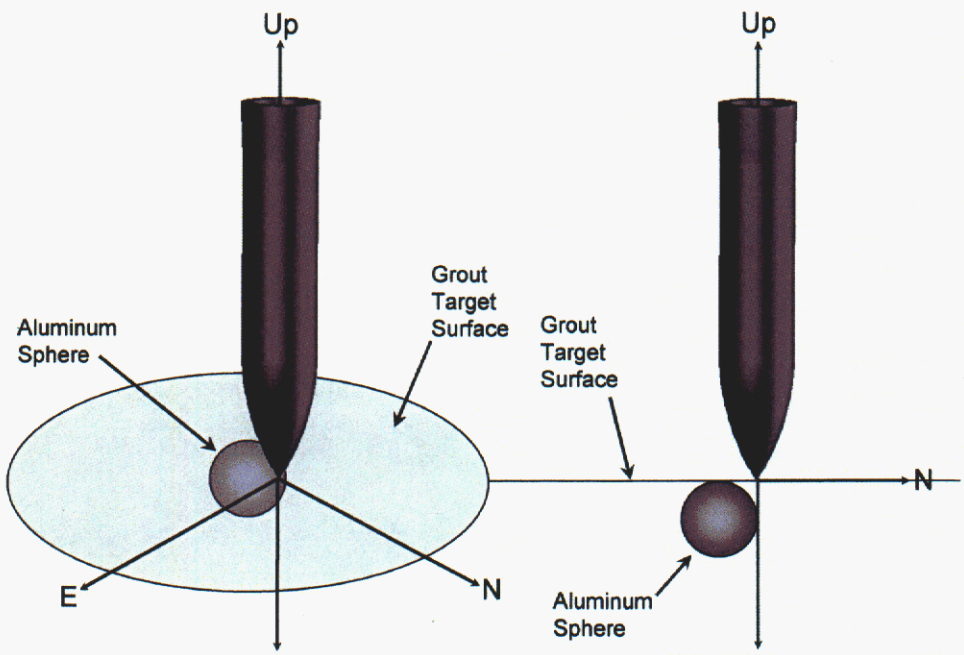

Figure 5. Nominal Impact Geometry for LSG-4 [14]

Table 1. LSG-1 Initial Impact Conditions [14]

Parameter	Value
Inclusion	None
Matrix	Low-Strength Grout
Impact Velocity, West Camera	652.50 ± 1.90 fps (Nose North)
Angle of Attack, West Camera	0.24° ± 0.08° (Nose North)
Impact Angle (Obliquity), West Camera	0.45° ± 0.22° (Nose North)
Impact Velocity	— (Camera failed to operate)
Angle of Attack	— (Camera failed to operate)
Impact Angle (Obliquity), South Camera	0.11° ± 0.22° (Nose East)
Impact Point, South Camera	0.047" ± 0.031" West of target center
Impact Point, West Camera	1.447" ± 0.031" North of target center

Table 2. LSG-2 Initial Impact Conditions [14]

Parameter	Value
Inclusion	Indiana Limestone, 3"-diameter rod, 12" long. Rod was 0.25" below top surface of grout.
Matrix	Low-Strength Grout
Impact Velocity, West Camera	660.84 ± 1.90 fps (Nose South)
Angle of Attack, West Camera	0.24° ± 0.08° (Nose South)
Impact Angle (Obliquity), West Camera	0.34° ± 0.22° (South side, Nose North) 0.22° ± 0.22° (North side, Nose North)
Impact Velocity, South Camera	662.87 ± 1.93 fps (Nose East)
Angle of Attack, South Camera	0.32° ± 0.08° (Nose East)
Impact Angle (Obliquity), South Camera	0.22° ± 0.22° (East side, Nose East) 0.34° ± 0.22° (West side, Nose East)
Impact Point, South Camera	0.144" ± 0.031" West of target center
Impact Point, West Camera	1.397" ± 0.031" North of target center

Table 3. LSG-3 Initial Impact Conditions [14]

Parameter	Value
Inclusion	Indiana Limestone, 3"-diameter cylinder, 12" long. Rod was 0.125" above top surface of grout.
Matrix	Low-Strength Grout
Impact Velocity, West Camera	662.78 ± 1.90 fps (Nose South)
Angle of Attack, West Camera	0.32° ± 0.08° (Nose South)
Impact Angle (Obliquity), West Camera	0.22° ± 0.22° (South side, Nose North) 0.0° ± 0.22° (North side, Nose North)
Impact Velocity, South Camera	660.28 ± 1.91 fps (Nose East)
Angle of Attack, South Camera	0.39° ± 0.08° (Nose East)
Impact Angle (Obliquity), South Camera	0.56° ± 0.22° (East side, Nose West) 0.56° ± 0.22° (West side, Nose West)
Impact Point, South Camera	0.080" ± 0.031" West of target center
Impact Point, West Camera	1.530" ± 0.031" North of target center

Table 4. LSG-4 Initial Impact Conditions [14]

Parameter	Value
Inclusion	6061 T6 Aluminum, 3"-diameter sphere. Top of sphere was 0.0625" above top surface of grout.
Matrix	Low-Strength Grout
Impact Velocity, West Camera	646.89 ± 1.88 fps (Nose South)
Angle of Attack, West Camera	0.32° ± 0.08° (Nose South)
Impact Angle (Obliquity), West Camera	0.22° ± 0.22° (South side, Nose North) 0.22° ± 0.22° (North side, Nose North)
Impact Velocity, South Camera	650.80 ± 1.89 fps (Nose East)
Angle of Attack, South Camera	0.08° ± 0.08° (Nose East)
Impact Angle (Obliquity), South Camera	0.22° ± 0.22° (East side, Nose West) 0.12° ± 0.22° (West side, Nose West)
Impact Point, South Camera	0.111" ± 0.031" East of target center
Impact Point, West Camera	1.64" ± 0.031" North of target center

The first objective is to develop a baseline penetrability model for the low-strength grout in PENCURV. For modeling target material, PENCURV contains two algorithms: a hard rock algorithm and a soft rock algorithm. Three uniaxial compression tests were performed on samples of the grout matrix to assess its strength [15]. The results are summarized below.

Low-Strength Grout Matrix	Test 1	Test 2	Test 3
Unconfined Compressive Strength (MPa)	2.36	8.45	7.13
Density (g/cm^3)	1.9	1.89	1.93

The PENCURV authors recommend using the hard rock algorithm for targets with unconfined compressive strength (UCS) greater than 3.5 MPa and the soft rock algorithm for targets with UCS less than 3.5 MPa [8]. Since the above data straddle this cutoff, both methods were used and then compared with each other to determine the best algorithm to calculate penetration into the grout.

The hard rock algorithm was attempted first. Required inputs for this method are the target density and UCS. Two models were generated with this algorithm. One used a UCS of 2.4 MPa and the other a UCS of 8.0 MPa in accordance with the above data. Both models used a density of 1.9 g/cm^3. The modeled axial G-loading on the penetrator for both cases is shown in Figure 6 along with the actual test deceleration data. The test data shown, as well as all test data in this study, was filtered with a 1-KHz, low-pass, 4^{th} order Butterworth filter using PLOTDATA [16]. This filtering process introduces a time offset in the data. Therefore, the test data in Figure 6 and all subsequent graphs have been manually shifted to synchronize the start times of the PENCURV data and the test data.

For the soft rock algorithm, the only required input for the target material is the S-number. S-number is not tied to any standard material property. It is a unitless number that is simply used as a general description for a material's resistance to penetration. Materials that are more resistant to penetration have smaller S-numbers, and vice versa.

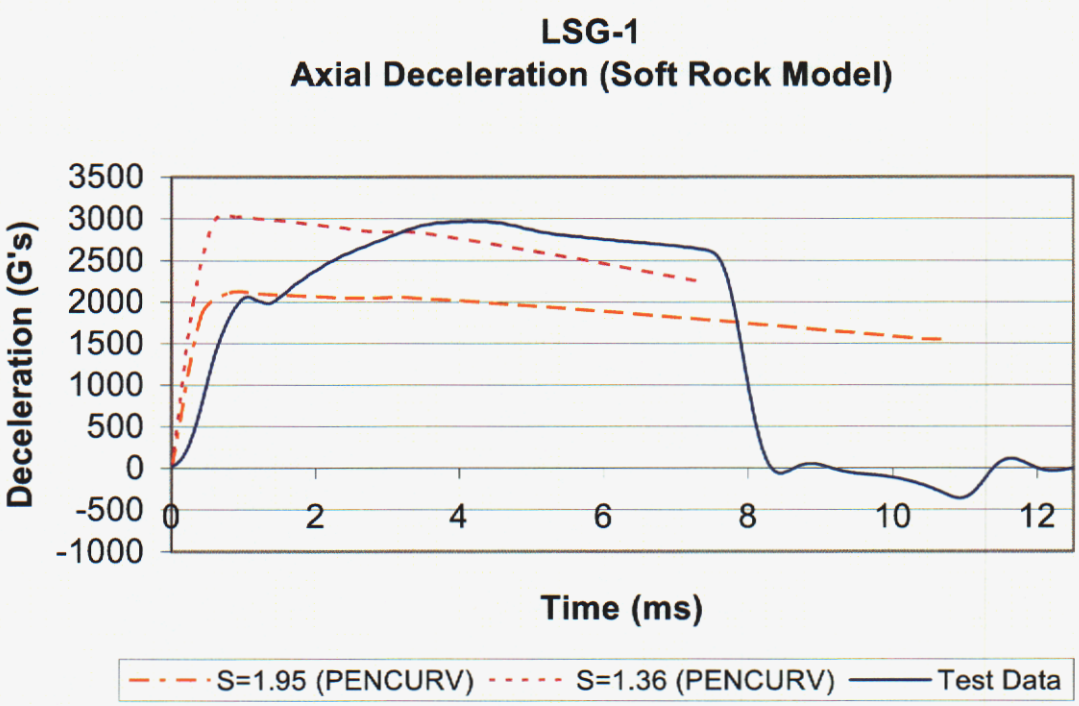

Figure 6. LSG-1 PENCURV Hard Rock Model

To use the soft rock model in PENCURV, a relationship must be drawn between S-number and UCS. Young [2] does this with the following empirical equation:

$$S = 0.085(F/W_1)^{0.3}(11\text{-}P)(t_c T_c)^{-0.06}(5000/f_c)^{0.3}$$

where

F = 20 for reinforced concrete or 30 for no reinforcement
W_1 = target width in penetrator calibers
P = volumetric percent rebar in concrete
t_c = cure time of concrete in years ($t_c \leq 1$)
T_c = thickness of target in penetrator calibers
f_c = UCS (psi) at test time

Using this equation, assuming a cure time of 3 months, and applying the UCS inputs of 2.4 MPa and 8.0 MPa, we get S = 1.95 and S = 1.36, respectively. Both of these models were generated and produced the results shown in Figure 7.

For all four of the models generated, the penetration depth was also calculated. The results are summarized in the table below.

		Hard Rock Model		Soft Rock Model	
	Test Data	UCS = 2.4 MPa	UCS = 8.0 MPa	S = 1.95	S = 1.36
Depth of Penetration	31.85 in.	51.59 in.	25.37 in.	41.66 in.	29.61 in.

The hard rock models in Figure 6 bracket the test data well when considering maximum deceleration, event duration and depth of penetration. While the 8 MPa hard rock model predicts the depth of penetration reasonably well, its peak axial deceleration is rather high and it dies off much quicker than the actual test data.

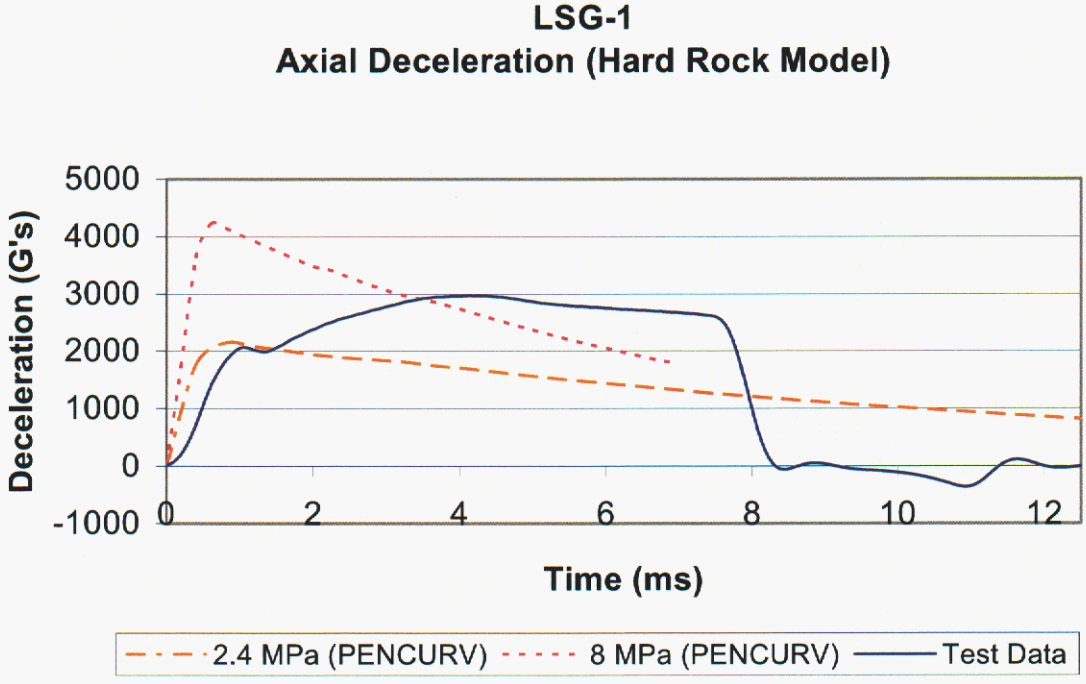

Figure 7. LSG-1 PENCURV Soft Rock Model.

On the other hand, the soft rock model (S = 1.36) is better on all counts. It predicts the depth of penetration well and its axial deceleration curve and event duration mirrors the test data rather closely. For this particular low-strength grout, then, the soft rock algorithm is better suited for modeling penetration scenarios. As a final calibration in preparation for LSG-2, 3 and 4, the S-number was varied until the model matched the actual depth of penetration (31.85 in.). This resulted in a best fit S-number of S = 1.47. The axial deceleration curve for this model is shown in Figure 8.

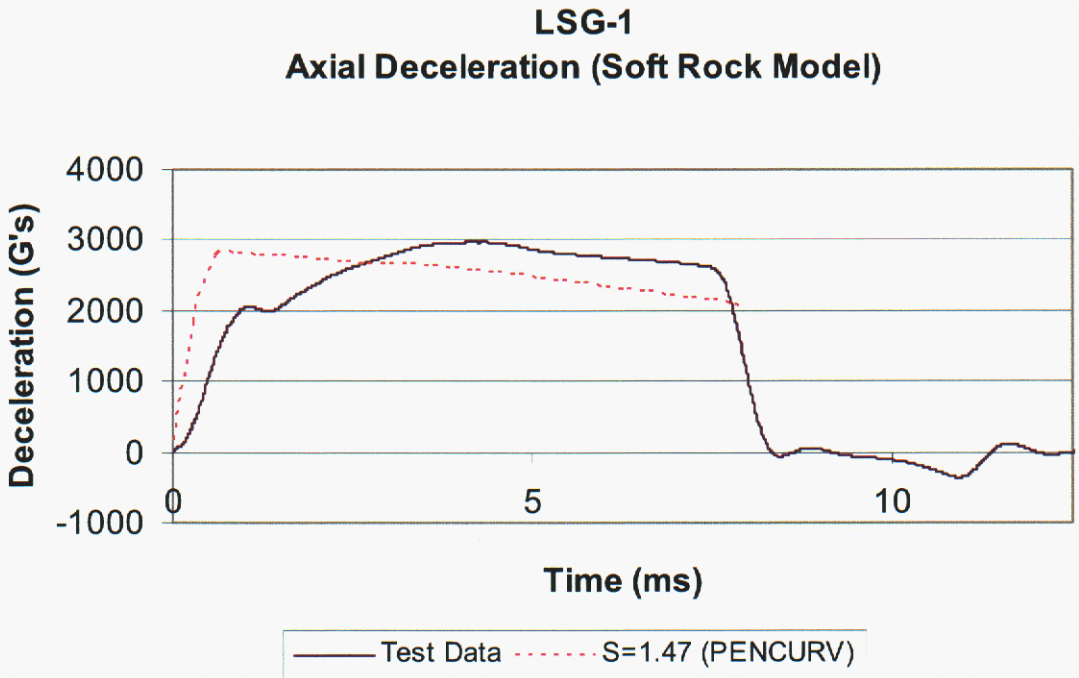

Figure 8. LSG-1 PENCURV Best Fit Model

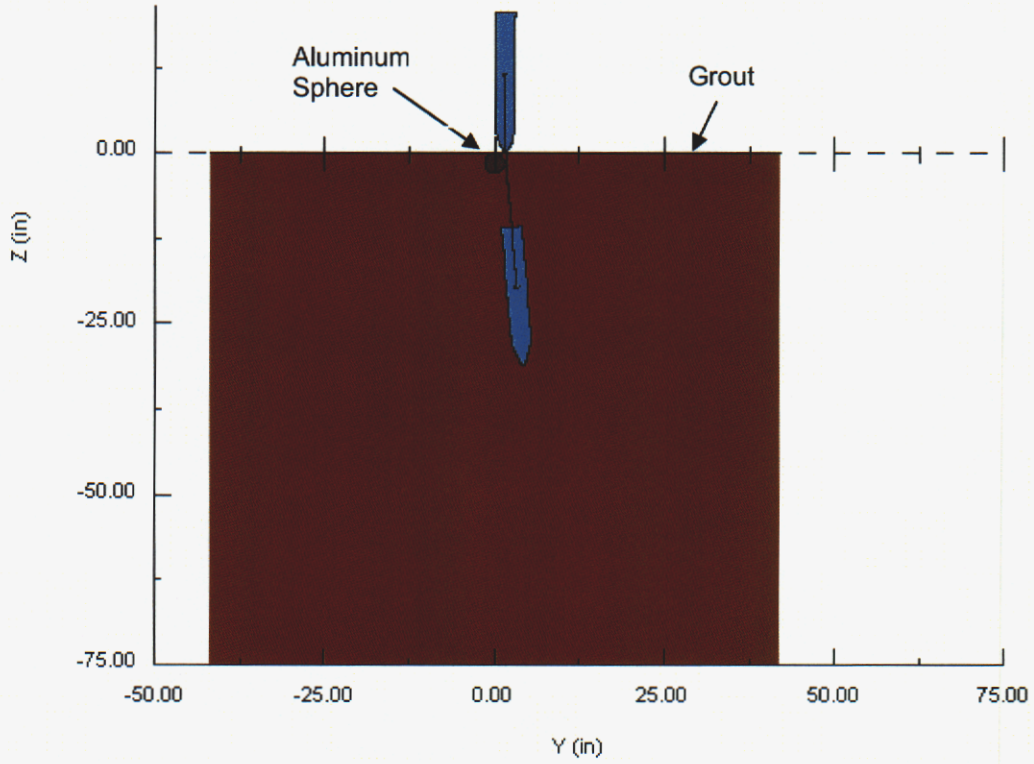

Figure 9. LSG-4 Event Geometry. Impact Velocity = 648.8 ft/s (197.8 m/s)

4. Modeling the Complex Targets

The preceding model for the low-strength grout can now be used in the target model for LSG-2, LSG-3, and LSG-4.

Consider first LSG-4. The material properties for the aluminum sphere must be added. PENCURV requires inputs of density and unconfined compressive strength. For the aluminum, the values input were a density of 2.7 g/cm^3 and a UCS of 290 MPa.

To permit modeling of LSG-4 in PENCURV, the obliquity angles from Table 4 had to be transformed to an Euler yaw angle (representing an azimuth from true North) and the impact angle (representing an elevation), to describe the orientation of the penetrator centerline. The results are tabulated below.

	Euler Yaw Angle	Impact Angle
LSG-4	37.69° West of North	180.28°

This data was incorporated into the PENCURV model along with the other required data from Table 4. Multiple data points in Table 4, such as obliquity, were averaged and uncertainties in the data were not considered for this simulation.

A cross-section of the predicted LSG-4 event can be seen in Figure 9. Figure 10 shows the axial, pitch and yaw G-loads predicted by PENCURV for LSG-4. In PENCURV, the pitch direction is defined as being orthogonal to the penetrator centerline in addition to being contained within the vertical plane containing the same centerline. Yaw is then orthogonal to both the pitch direction and the penetrator centerline. While the data in

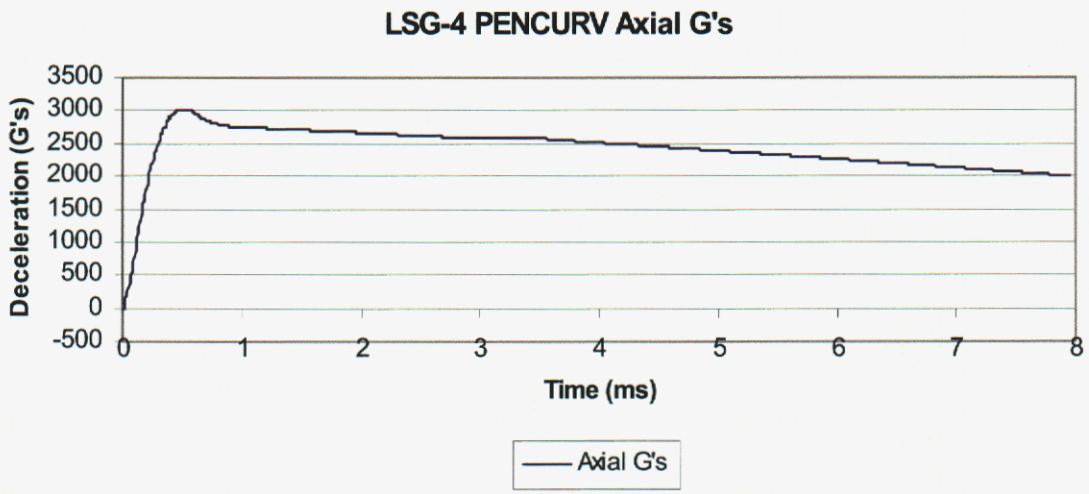

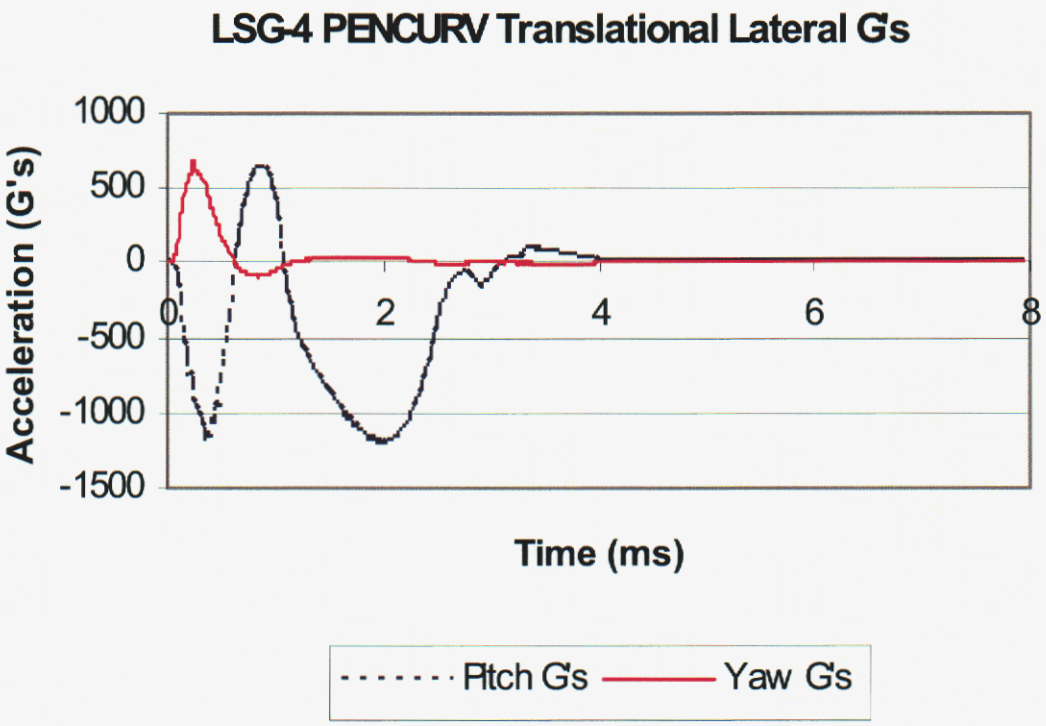

Figure 10. LSG-4 PENCURV G-Load Predictions

Figure 10 are informative, it is difficult to visualize the physical orientation since the pitch and yaw directions are constantly changing as the penetrator centerline changes orientation during the event.

A better way to look at the lateral acceleration data is to transform the pitch and yaw accelerations into their North-South and East-West components. While PENCURV does not perform this operation, it does generate the Euler yaw angle for each time step. Since this parameter represents the angle between true North and the projection of the pitch direction on a horizontal plane, it is straightforward to calculate these components. This has been done and is shown in Figure 11 for the LSG-4 model. These graphs are much

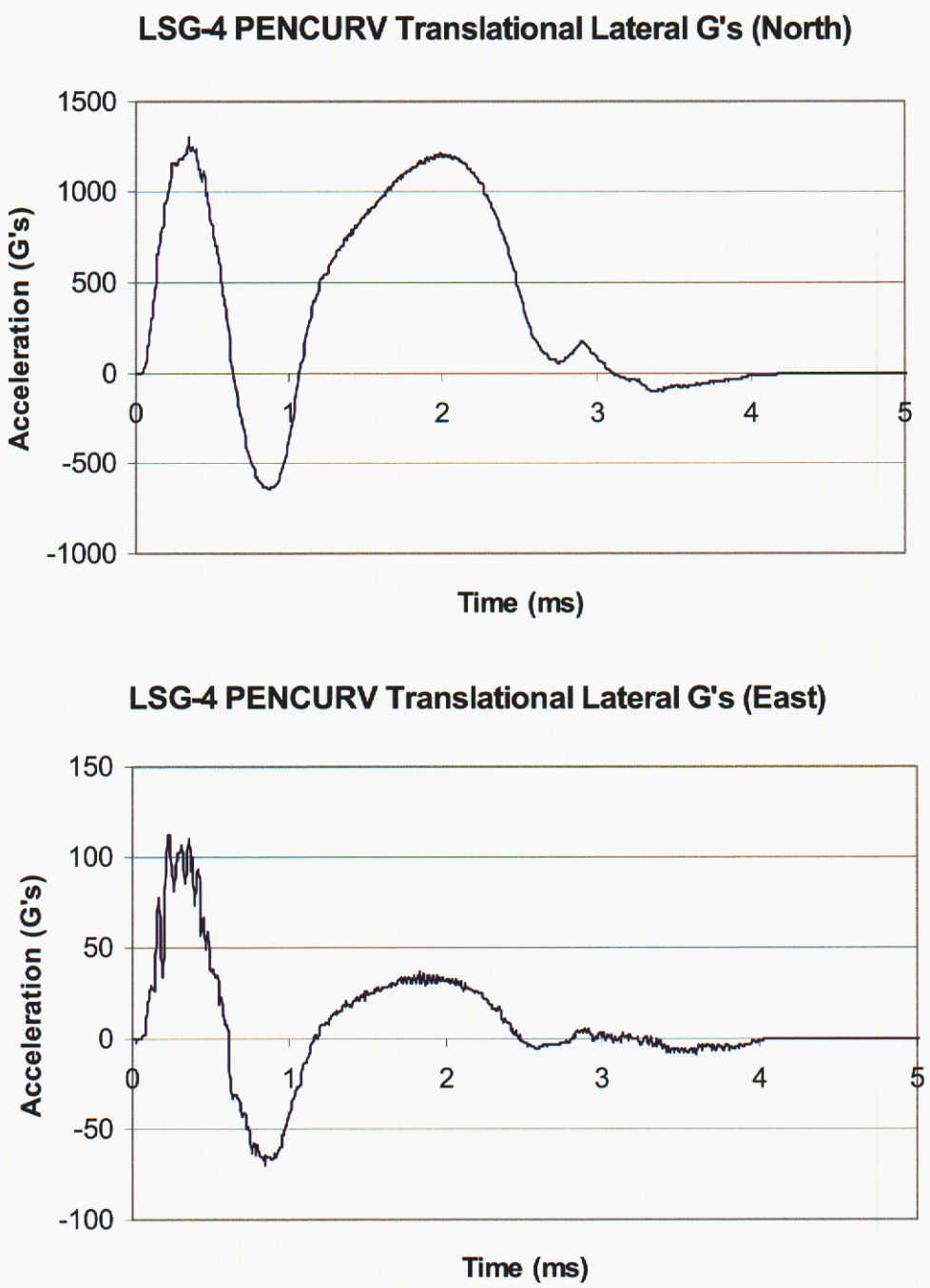

Figure 11. LSG-4 PENCURV North/East Translational Lateral G-Loads

more intuitive. The accelerations in the North-South direction are due to the penetrator bouncing off the aluminum sphere. The minor accelerations in the East-West direction are due primarily to the penetrator striking the sphere slightly east of its intended coordinate.

While the graphs in Figure 11 are insightful, they only provide part of the picture. PENCURV predicts only translational G-loading in the lateral direction. It does not directly estimate G-loading in the lateral direction due to rotation of the penetrator. In

problems such as LSG-4, this is a significant omission, as rotational acceleration can equal or exceed translational acceleration in the lateral direction over some periods of the event. While PENCURV does not calculate rotational accelerations, it does calculate angular velocity about the pitch axis. Therefore, a method to estimate rotational acceleration at the accelerometer is to calculate the derivative of the angular velocity data via a spreadsheet and multiply that by the accelerometer's moment arm (distance from the center of mass). This simple computation will give a good first-order approximation as long as the axis of rotation does not stray far from the penetrator's center of mass.

This technique was employed for the pitch angular velocity, with the results then added to the translational accelerations to arrive at total lateral accelerations at the accelerometers. While it would be more accurate to also perform this analysis on the yaw angular velocity, PENCURV does not generate this data in its output stream. The yaw angle and yaw rate that it does generate are effectively measures of rotation about the centerline of the penetrator, not the yaw axis. The predicted lateral G's, with rotational pitch acceleration added, are shown in Figure 12. The differences between Figures 11 and 12 are evident. Including the pitch rotation effectively doubles the lateral G-loading at the accelerometers in early time.

Since the angular positions of the accelerometers were not tracked for the penetration event, the accelerations from Figure 12 were combined to compute the magnitude of the total lateral acceleration for the event. The same operation was performed on the accelerometer test data. The magnitudes could then be compared directly with each other.

In addition to the PENCURV modeling done here, Hollenshead [17] has performed some preliminary modeling for LSG-4 using Zapotec. His analysis incorporated a Lagrangian penetrator and aluminum sphere built in Pronto 3D, and an Eulerian grout matrix built in CTH. The material model used for the grout was developed by Kipp [18] and incorporates volumetric, deviatoric, and fracture response to impact stress. For this calculation, the CTH grid spacing in the center of the target was only 0.295 inches (0.75 cm). For follow-on work, plans include reducing this grid spacing to try and produce higher fidelity models. Despite this fact, his results are included here for comparative purposes.

The calculated models for PENCURV and Zapotec are plotted, along with the actual test data, in Figure 13 for LSG-4. For this test, it is worth noting that the aluminum sphere was ejected from the grout target during the penetration event.

The same analysis can now be applied to LSG-2 and LSG-3. This time, the Indiana limestone material properties must be added. Frew, *et al.* [19] carried out extensive penetration testing of the identical limestone used in these tests. He defined a nominal limestone density of 2.3 g/cm^3 and a nominal UCS of 60 MPa. These values were used for all LSG-2 and LSG-3 modeling.

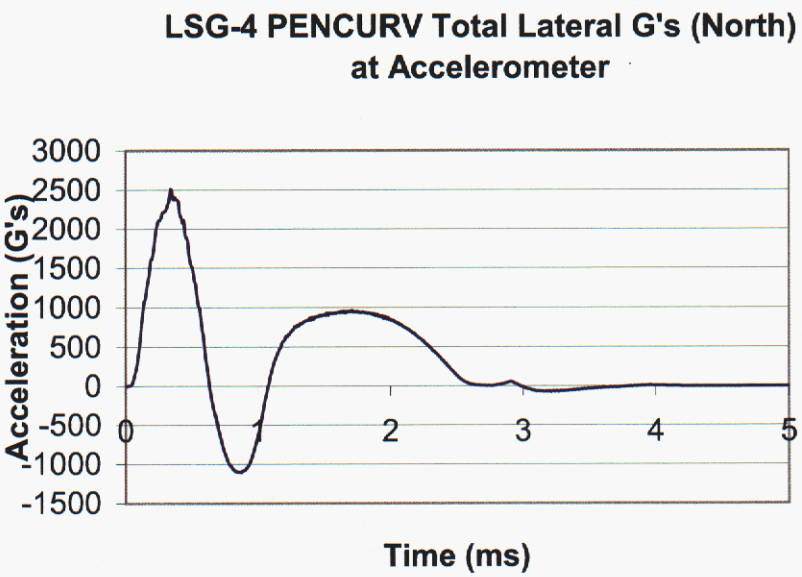

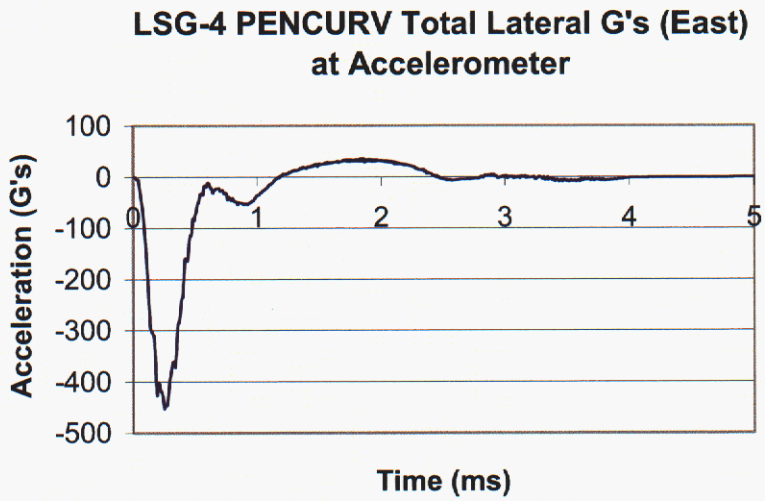

Figure 12. LSG-4 PENCURV North/East Total Lateral G-Loads

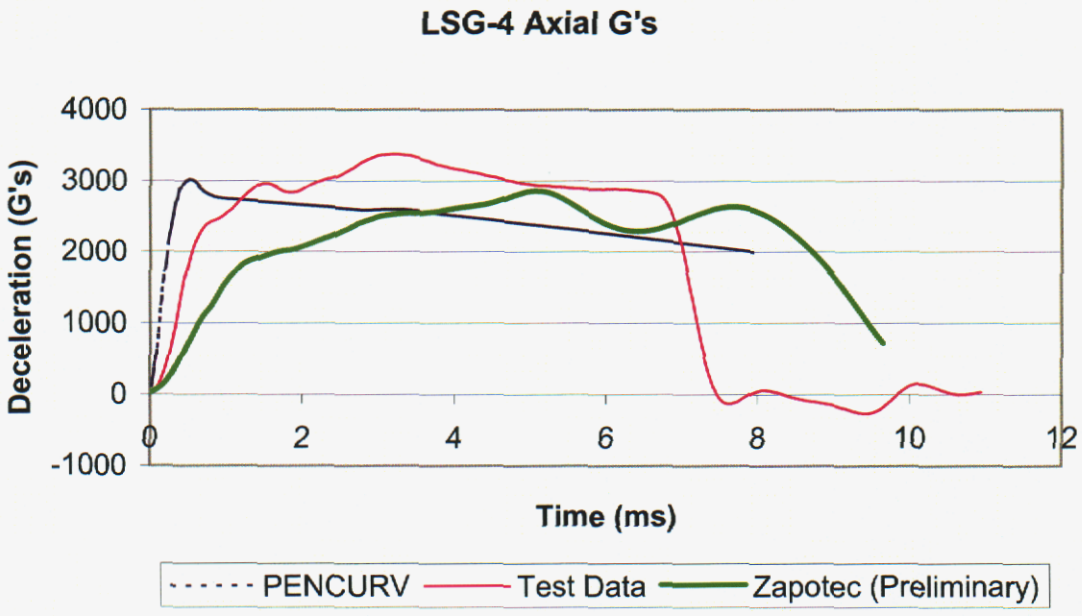

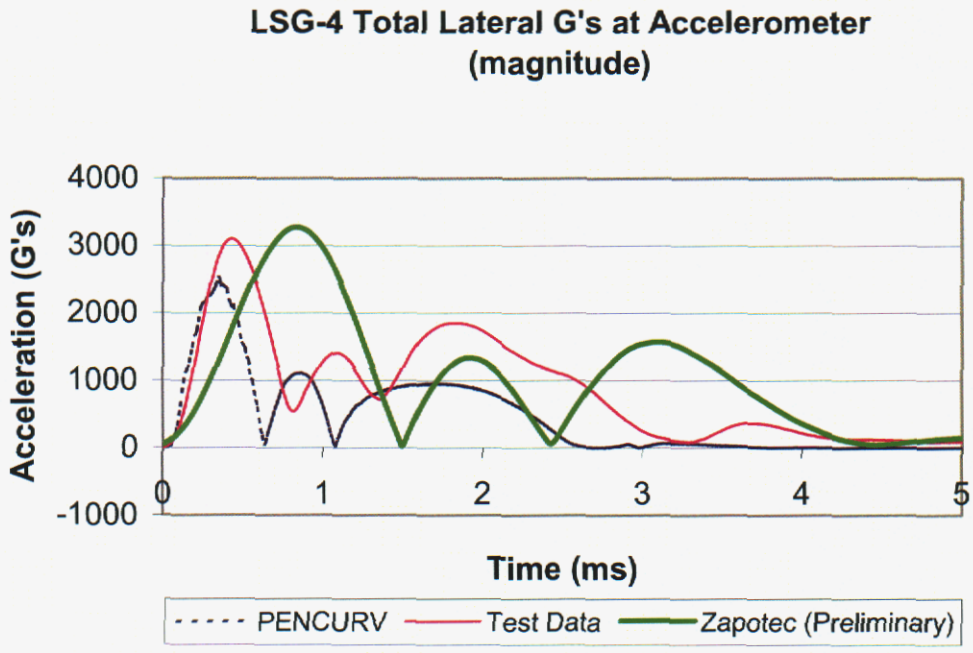

Figure 13. LSG-4 Predictions and Test Data

As in LSG-4, the obliquity angles from Tables 2 and 3 must be transformed to Euler yaw angle and impact angle. The results for LSG-2 and LSG-3 are tabulated below.

	Euler Yaw Angle	Impact Angle
LSG-2	45.00° East of North	180.40°
LSG-3	78.89° West of North	180.57°

These data were incorporated into the PENCURV models with the other required data from Tables 2 and 3. As before, multiple data points in Tables 2 and 3, such as obliquity, were averaged and uncertainties in the data were not considered for these simulations.

A cross-section of the predicted LSG-3 event can be seen in Figure 14. Figure 15 shows the axial G-loading predicted by PENCURV for LSG-2 and LSG-3. After 0.6 ms, the models are almost identical. In early time (Figure 15), LSG-2 is showing slightly higher G-loading. This result is intuitive since LSG-2 impacted the target 0.133 inches (0.338 cm) South of LSG-3, thereby striking the harder limestone cylinder more directly. In fact, the tip of the penetrator passes slightly through the volume of the limestone in LSG-2. This can be seen visually in Figure 16. This particular penetration geometry also gives rise to the slight spike in the LSG-2 model at about 0.25 ms (Figure 15). In Figure 16, the circle represents a cross-section of the limestone cylinder, the two penetrator outlines represent its position at the times that span the spike, and the blue line represents the trajectory of the nose tip.

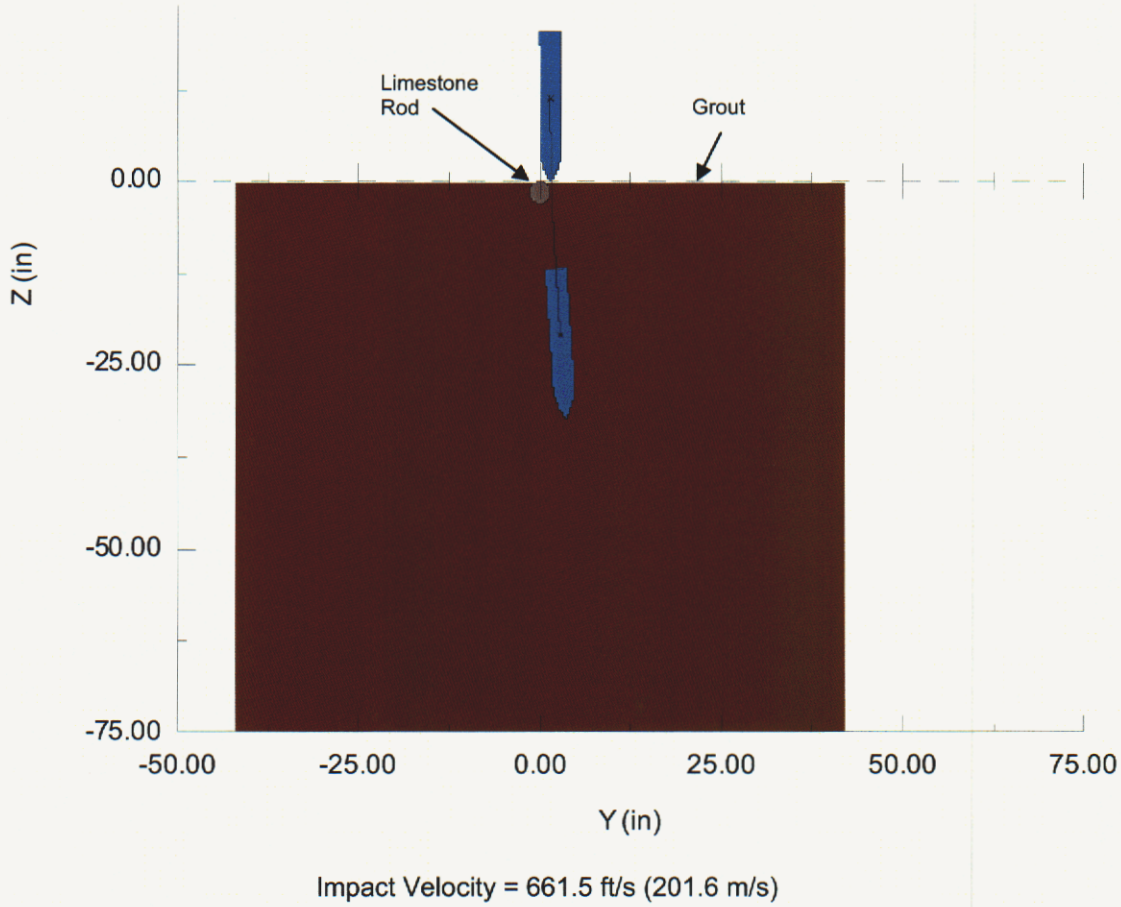

Figure 14. LSG-3 Event Geometry

The spike in the LSG-2 model can likely be attributed to PENCURV's method for calculating stress on the penetrator. For each element on the penetrator, two "damage vectors" are defined which in turn give rise to two stress calculations on the element. One vector is normal to the element, and the other is parallel to the velocity of the element. Stress, for each vector, is evaluated as a weighted average of the length of the damage vector contained in the various target materials. The harder the material is, the higher the stress. Once they are computed, the normal components of the two stresses are compared to each other and the smaller one is used for the subsequent iteration.

The actual computed stress values are buried within the algorithm and cannot be accessed by the user. However, a plausible explanation for this "spike" is that the two stresses evaluated for the elements near the nose cross over between about 0.22 ms and 0.29 ms. In other words, one can imagine from the geometry in Figure 16 that the velocity-oriented stress is less than the normal stress for elements near the nose from 0.22 ms to 0.29 ms, and greater than the normal stress at all other times. It would follow that, for elements near the nose, the velocity-oriented stress is used between 0.22 ms and 0.29 ms and the normal stress is used everywhere else. In any case, this anomaly is minor and does not preclude further analysis of the simulation results.

The PENCURV pitch and yaw lateral acceleration predictions can be seen in Figure 17. Like the axial G's, the lateral G's are slightly greater for LSG-2 than LSG-3. This is again due to the penetrator in LSG-2 striking the limestone more directly. The spike seen in LSG-2 around 0.25 ms is due to the same phenomenon that was mentioned earlier.

The same technique used for LSG-4 of transforming lateral accelerations to North-South and East-West directions and including the rotational pitch acceleration was employed here for LSG-2 and 3. This data is plotted, along with the actual test data, in Figure 18 for LSG-2 and Figure 19 for LSG-3.

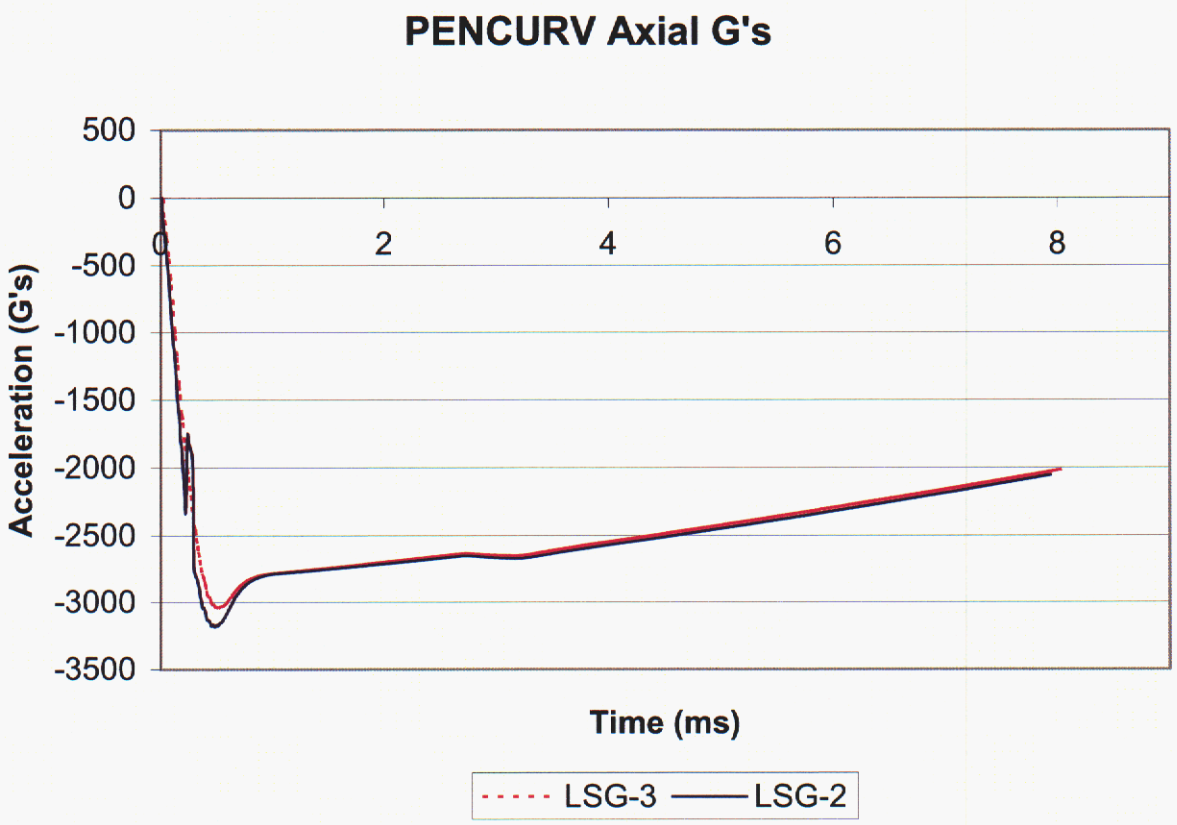

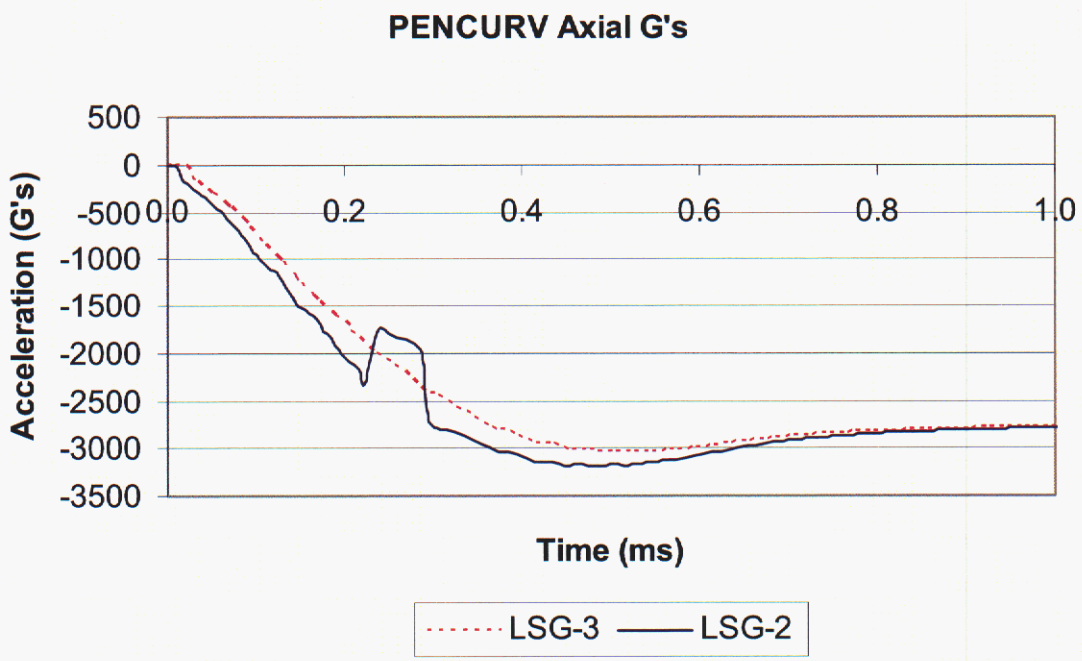

Figure 15. LSG-2 and 3 PENCURV Axial G-Load Predictions

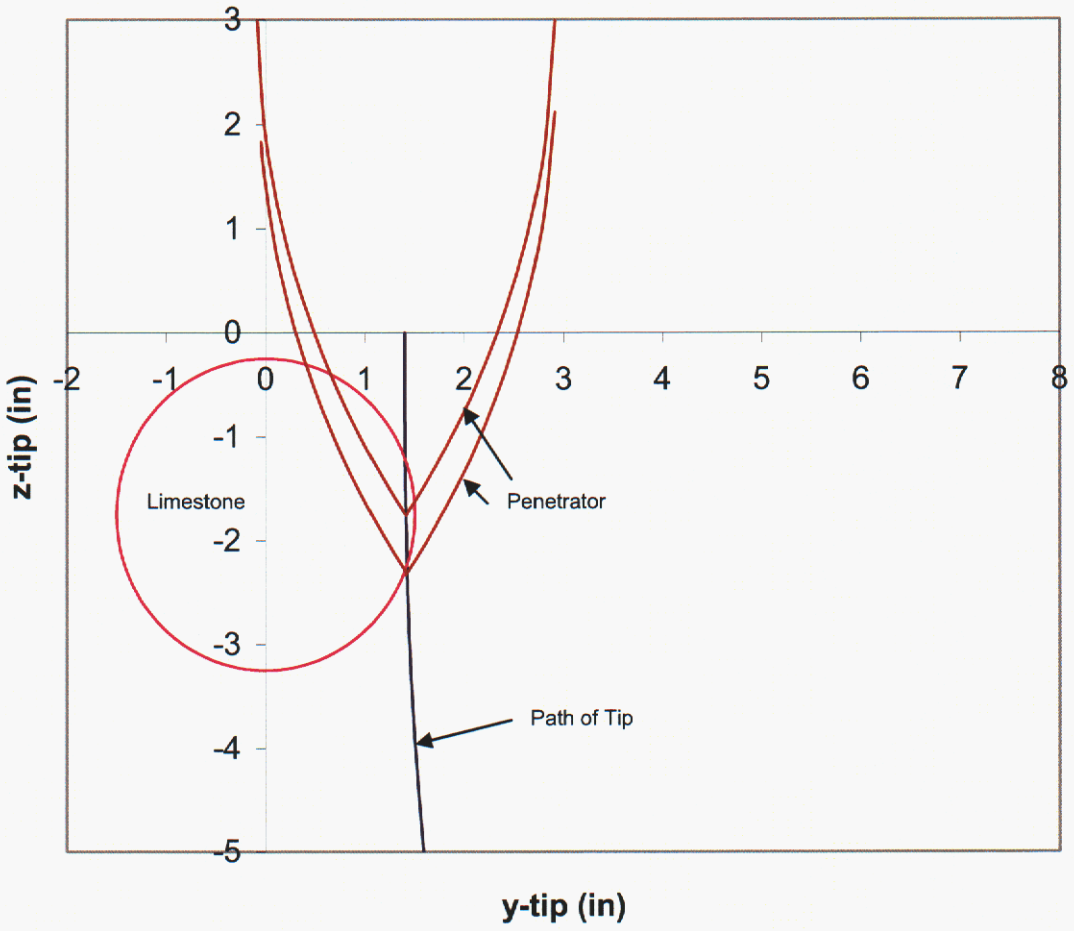

Figure 16. LSG-2 Limestone/Penetrator Geometry

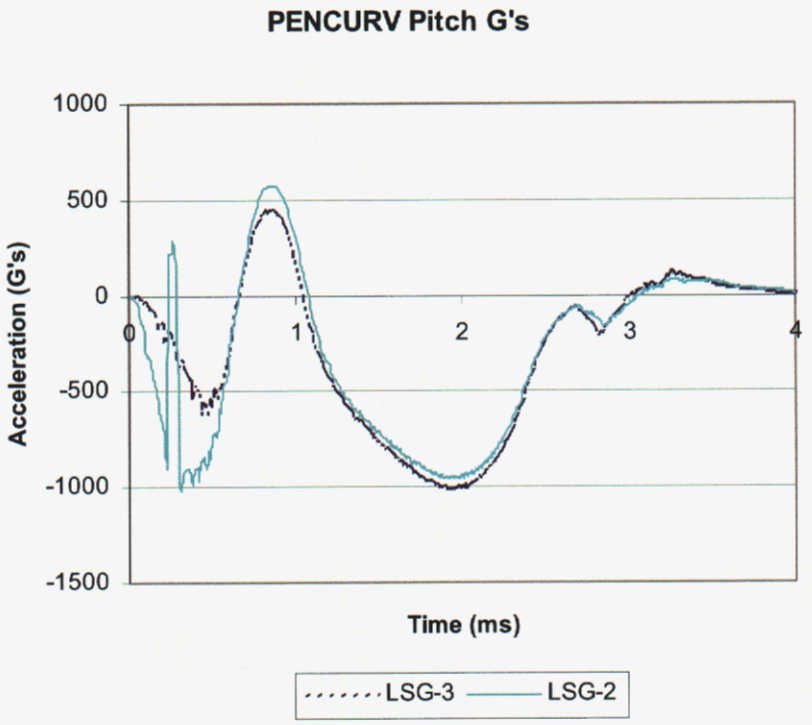

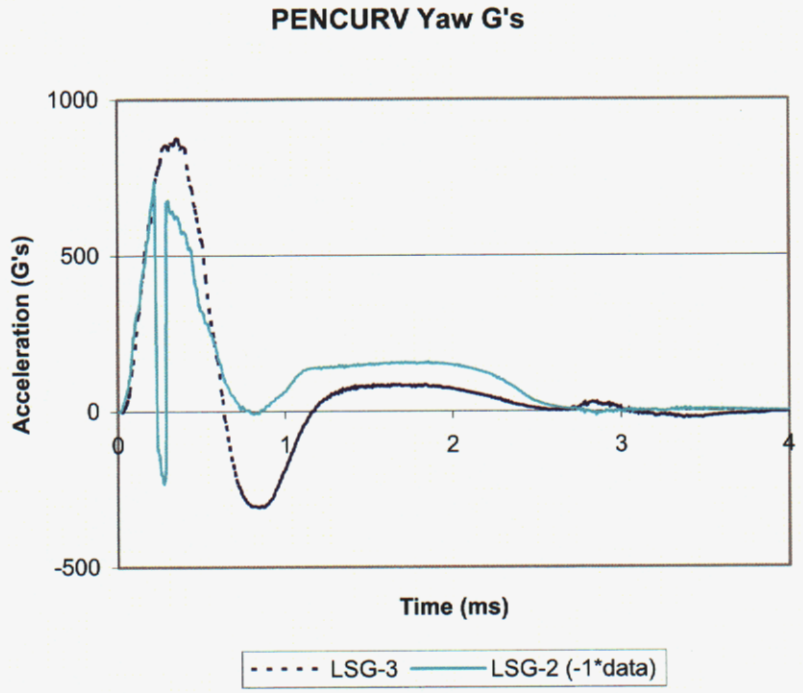

Figure 17. LSG-2 and 3 PENCURV Lateral G-Load Predictions

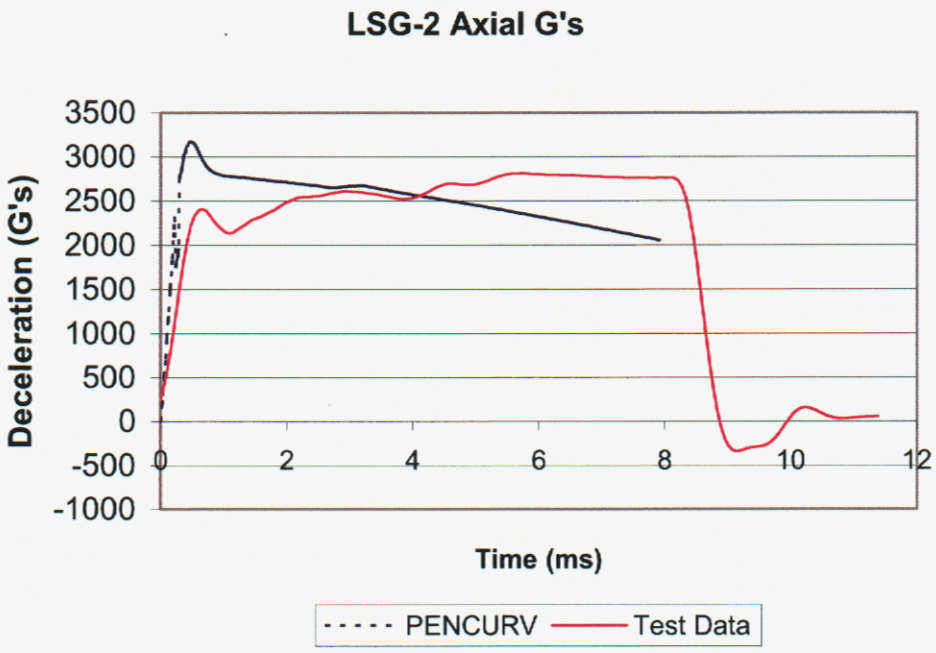

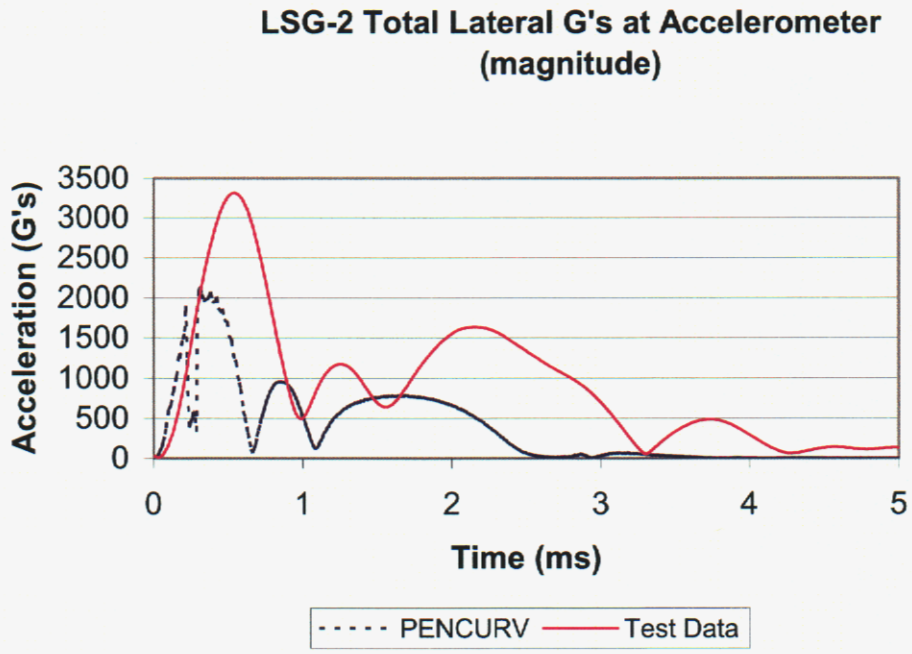

Figure 18. LSG-2 Predictions and Test Data

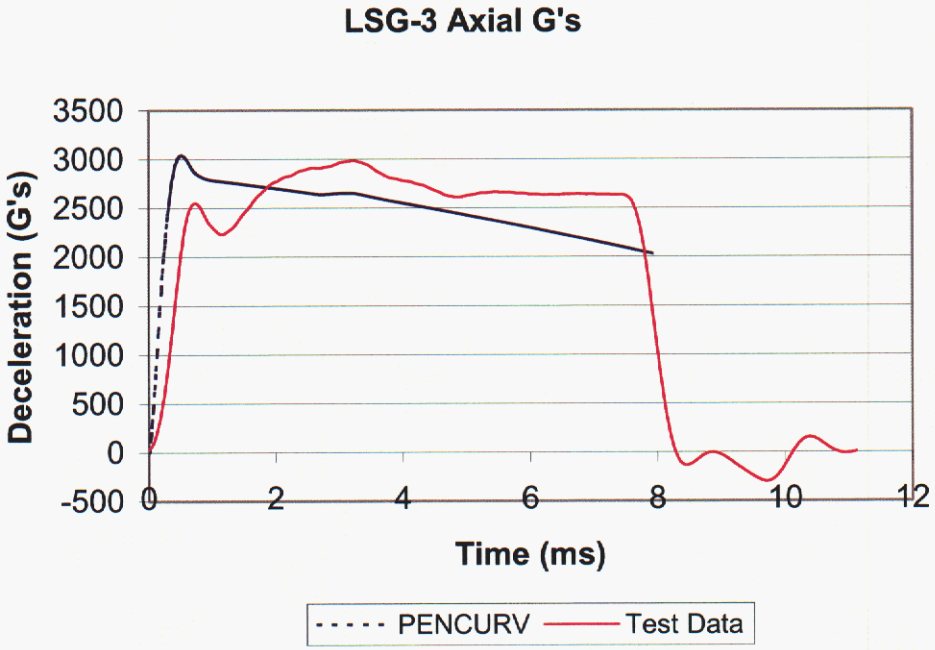

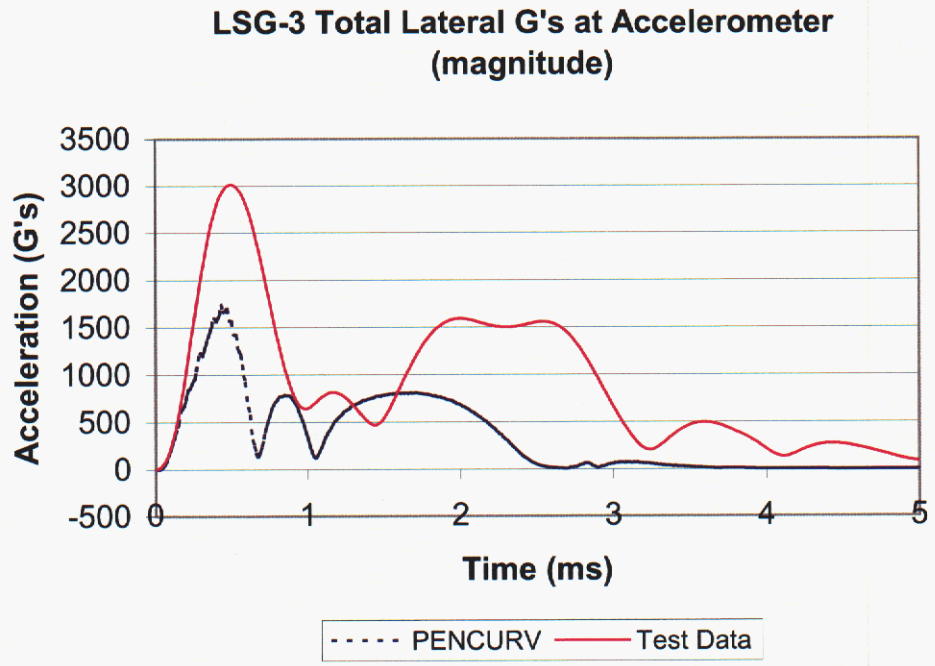

Figure 19. LSG-3 Predictions and Test Data

5. Discussion

Looking at the LSG-4 results, Figure 13 reveals that both PENCURV and Zapotec are predicting axial deceleration curves that vary noticeably from the test data. However, the maximum predicted axial deceleration is within 15% of the data for the preliminary Zapotec results and 10% for the PENCURV results. While PENCURV does not capture all the details evident in the test data, it does model a relatively flat deceleration history that is a fairly good first order approximation of the actual event, including the event termination time.

Looking at the lateral accelerations for LSG-4 (Figure 13), both models emulate the general shape of the test data relatively well, but Zapotec does a better job of matching the observed maximum amplitude of the test data. The preliminary Zapotec results are within 6% of the test data maximum amplitude whereas the PENCURV results are within 18%. This graph shows a weakness in the PENCURV methodology. While rotational pitch acceleration can be manually calculated via the method described earlier, PENCURV does not generate the required data to manually compute rotational yaw acceleration. The impact of neglecting this contribution to lateral acceleration depends on the Euler yaw angle as defined in the penetrator initial conditions. If the Euler yaw angle is close to zero, the impact will be negligible. Conversely, the impact of this omission will be greatest when the Euler yaw angle is ±90°. Since this parameter was 37.7° for LSG-4, one can expect a PENCURV prediction to be somewhat lower than the actual test data, particularly in early time. The results shown in Figure 13 are in line with these projections.

Although LSG-2 and LSG-3 had a limestone cylinder in place of an aluminum sphere, the axial deceleration histories were quite similar to LSG-4 for both the test data and the PENCURV models (Figures 18 and 19). Again, there is a noticeable difference between the data and the models, but the maximum amplitudes are within 13% of the test data maximum for LSG-2 and 3% for LSG-3. PENCURV is quite accurate for the event duration time in LSG-3. But in LSG-2, where the penetrator hits the limestone more directly, PENCURV seems to overestimate the limestone's resisting stress, thus producing a slower penetrator that now stops about 0.3 ms early.

Like LSG-4, the LSG-2 and LSG-3 lateral accelerations capture the general shape of the test data well (Figures 18 and 19). There is a discrepancy, however, between the maximum acceleration values. The peak lateral accelerations in the PENCURV models are only within 36% of the test data for LSG-2 and 42% for LSG-3. As with LSG-4, this is at least partially due to the omission of the rotational yaw acceleration. These discrepancies are also in line with the initial Euler yaw angles of -45° for LSG-2 and 79° for LSG-3. An additional reason that these discrepancies may be so high compared with LSG-4 is that the aluminum sphere was ejected during the LSG-4 event, thus eliminating a strong lateral stress load early in the event. Since PENCURV cannot model the ejection of material, the omission of the rotational yaw acceleration was partially offset by the increased G-loading of a sphere that was still locked in place in the PENCURV model. A

final source of uncertainty is the limestone model itself. If the assumed UCS of 60 MPa is low, this would be reflected in lateral acceleration models which are also low.

As a final comparison, the velocities and displacements in the –Z-direction (into the target) are shown in Figures 20 and 21 for LSG-4, LSG-2, and LSG-3 respectively. The velocities and the displacements for the test data were calculated by integrating the acceleration data. Overall, the models match the data very well and serve to validate PENCURV for adequately modeling these parameters.

This study shows that when accurate characterization of maximum G-loads is of primary interest, PENCURV results are mixed. In the axial direction, PENCURV appears to be an acceptable program for conducting broad scoping studies over a wide range of complex target geologies and geometries. For the lateral direction however, while maximum G-loads can be estimated, they will likely be too low due to the fact that only translational accelerations are computed directly. A method has been proposed for manually including rotational acceleration in the pitch direction, but the revised lateral accelerations will still likely be low because yaw rotational acceleration cannot be computed with the data currently output by PENCURV.

These shortcomings could be addressed in a future version of the PENCURV program. First, the algorithm could be modified to calculate the axis of rotation for the penetrator. Then, moment arms could be calculated for a series of user-defined tracer points at every time step. These moment arms could then be used to estimate the rotational acceleration for all the tracer points in both the pitch and yaw directions. Summing these rotational accelerations with the translational accelerations currently produced would provide a much more robust method of estimating lateral G-loadings for any particular place on the penetrator.

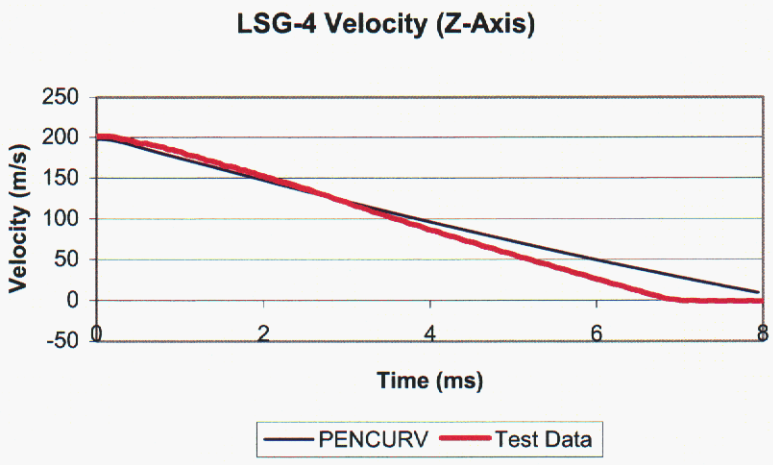

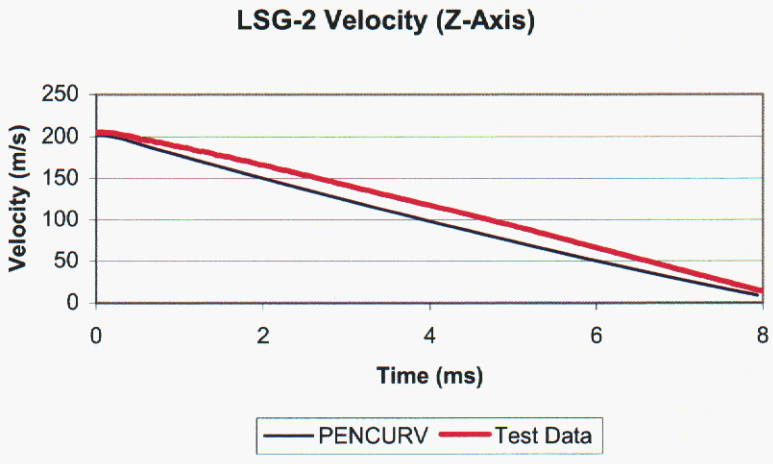

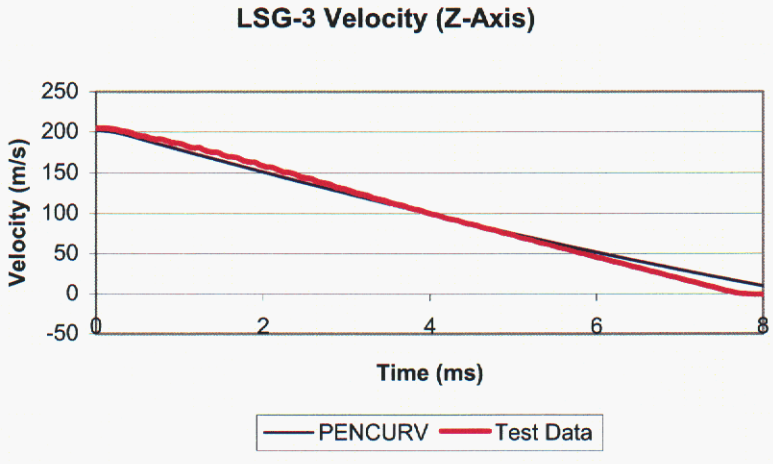

Figure 20. LSG-4, 2 and 3 Velocity Predictions and Test Data

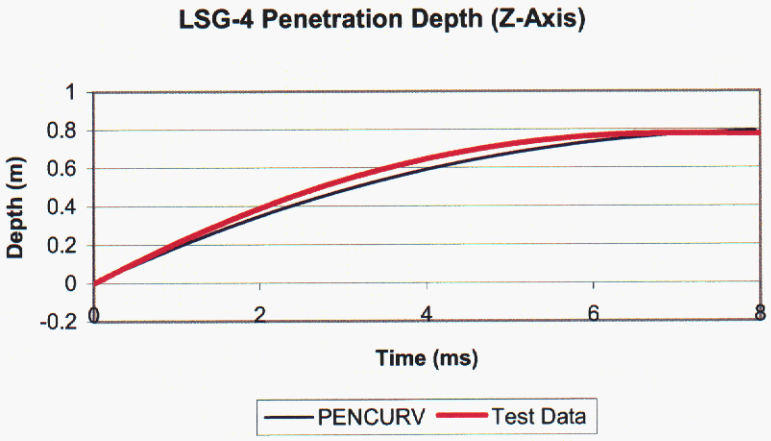

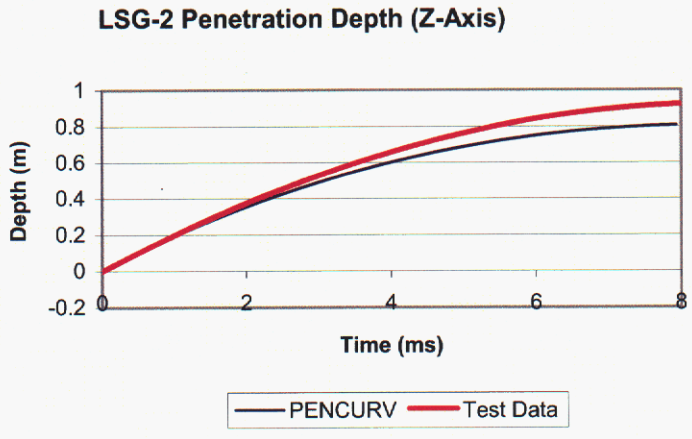

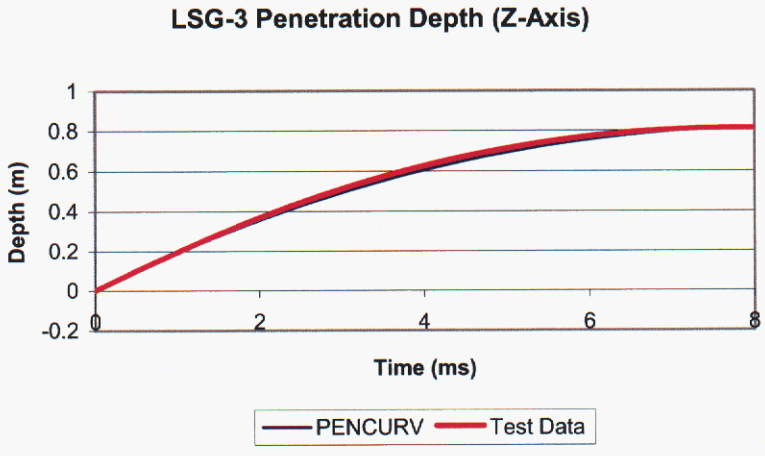

Figure 21. LSG-4, 2 and 3 Depth Predictions and Test Data

6. Summary

While programs such as Zapotec have been demonstrated as valuable modeling tools for penetration events, the simulations may take several days to execute on one of the massively parallel machines at either Sandia National Laboratories or other facilities. The time and expense required to complete these simulations become prohibitive when a large number of different geologic environments and geometries need to be investigated. For these types of studies, other modeling platforms must be considered.

PENCURV, which can model a typical event in only a few seconds on a PC, is a promising alternative. It is true that a PENCURV model has less fidelity than a program like Zapotec since it uses empirically derived stress equations and assumes a rigid penetrator. But if enhancements are made in the PENCURV program to model the lateral accelerations due to penetrator rotation for a series of user defined tracer points, it could be a valuable tool for getting first order solutions to a wide variety of problems. Armed with this information, high value assets can then be optimized by refining the high fidelity analysis and field testing that will be required to demonstrate the viability of the LDRD project and other systems.

7. References

1. Young, C. W., "The Development of Empirical Equations for Predicting Depth of an Earth Penetrating Projectile", SC-DR-67-60, Sandia National Laboratories, Albuquerque NM, May 1967.

2. Young, C. W., "Penetration Equations", SAND97-2426, Sandia National Laboratories, Albuquerque NM, October 1997.

3. Young, C. W., "Empirical Equations for Predicting Penetration Performance in Layered Earth Materials for Complex Penetrator Configurations", SC-DR-72-0523, Sandia National Laboratories, Albuquerque NM, December 1972.

4. Young, C. W., "Equations for Predicting Earth Penetration by Projectiles: An Update", SAND88-0013, Sandia National Laboratories, Albuquerque NM, July 1988.

5. Forrestal, M. J., *et al.*, "An Empirical Equation for Penetration Depth of Ogive-Nose Projectiles into Concrete Targets", SAND92-1948C, Sandia National Laboratories, Albuquerque NM, 1992.

6. Gardner, D. R., "Project Overview", Presented at the External Advisory Board Meeting for the LDRD "Near Real-Time Site Characterization for Assured Hard Deeply Buried Target (HDBT) Defeat", Sandia National Laboratories, Albuquerque NM, March 2004.

7. Young, C. W., "Simplified Analytical Model of Penetration with Lateral Loading – User's Guide", SAND98-0978, Sandia National Laboratories, Albuquerque NM, May 1998.

8. Adley, M. D., *et al.*, "Methodology and User's Guide for PENCURV+ Version 1.0", ERDC/GSL TR-03-2, US Army Corps of Engineers, Vicksburg MS, February 2003.

9. McGlaun, J. M., "CTH: A Three-Dimensional Shock Wave Physics Code", SAND89-0607C, Sandia National Laboratories, Albuquerque NM, 1989.

10. Bell, R. L., *et al.*, "CTH User's Manual and Input Instructions", Sandia National Laboratories, Albuquerque NM, July 2003.

11. Taylor, L. M. and Flanagan, D. P., "PRONTO 3D–A Three-Dimensional Transient Solid Dynamics Program", SAND87-1912, Sandia National Laboratories, Albuquerque NM, April 1998.

12. Bessette, G. C., *et al.*, "Zapotec: A Coupled Eulerian-Lagrangian Computer Code, Methodology and User Manual, Version 1.0", SAND2003-3097, Sandia National Laboratories, Albuquerque NM, October 2003.

13. Frew, D. J., "Results of Instrumented Penetration Experiments into Concrete Targets", Sandia National Laboratories, Albuquerque NM, June 2001.

14. Gardner, D. R., "Initial Conditions for the September 'Complex Target' Penetration Tests", unpublished memo, Sandia National Laboratories, Albuquerque NM, November 2003.

15. Lee, M. Y., personal communication, Sandia National Laboratories, Albuquerque NM, January 2004.

16. "PLOTDATA User Manual, Version 2.0", Explosive Projects/Diagnostics, Sandia National Laboratories, Albuquerque NM.

17. Hollenshead, J. T., personal communication, Sandia National Laboratories-California, Livermore CA, March 2004.

18. Kipp, M. E., "Lightweight Concrete CTH Model – Normal Impact Results", unpublished memo, Sandia National Laboratories, Albuquerque NM, December 2003.

19. Frew, D. J., *et al.*, "Penetration Experiments With Limestone Targets and Ogive-Nose Steel Projectiles", *Journal of Applied Mechanics*, Vol. 67, December 2000.

DISTRIBUTION

1 MS 0321
William J. Camp, 09200

1 MS 0318
Paul Yarrington, 9230

10 MS 0316
David R. Gardner, 9233

1 MS 0482
Ed R. Hoover, 2131

1 MS 0482
John L. Sichler, 2131

1 MS 0572
Eric P. Chael, 5736

1 MS 0750
Gregory J. Elbring, 6116

1 MS 0751
Laurence S. Costin, 6117

1 MS 9401
Jeromy T. Hollenshead, 8728

1 MS 0372
Joseph Jung, 9127

1 MS 0372
Donald B. Longcope, 9127

1 MS 0378
Gregory C. Bessette, 9232

1 MS 0370
Marlin E. Kipp, 9232

1 MS 0817
Courtenay T. Vaughan, 9232

1 MS 1221
John C. Hogan, 15100

1 MS 0859
K. Terry Stalker, 15351

1 MS 0844
Robert J. Fogler, 15352

1 MS 1160
Douglas A. Dederman, 15412

1 MS 1160
Danny J. Frew, 15412

1 MS 1160
Robert T. Gilchrist, 15412

1 MS 1138
Central Technical Files, 8945-1

2 MS 0899
Technical Library, 9616